Since January 2020 Elsevier has created a COVID-19 resource centre with free information in English and Mandarin on the novel coronavirus COVID-19. The COVID-19 resource centre is hosted on Elsevier Connect, the company's public news and information website.

Talanta 248 (2022) 123630

Contents lists available at ScienceDirect

Talanta

journal homepage: www.elsevier.com/locate/talanta

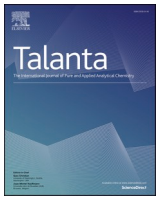

A paper-based optical sensor for the screening of viruses through the cysteine residues of their surface proteins: A proof of concept on the detection of coronavirus infection

Mahnaz D. Gholami [a], Kristyan Guppy-Coles [a], Serena Nihal [a], Daman Langguth [b,c], Prashant Sonar [a,d,e], Godwin A. Ayoko [a,d], Chamindie Punyadeera [f,g], Emad L. Izake [a,d,e,*]

[a] School of Chemistry and Physics, Faculty of Science, Queensland University of Technology (QUT), Brisbane, QLD, 4000, Australia
[b] Department of Clinical Immunology and Allergy, Wesley Hospital, Brisbane, QLD, 4066, Australia
[c] Department of Immunology, Sullivan Nicolaides Pathology, QLD, 4006, Australia
[d] Centre for Materials Science, Queensland University of Technology (QUT), Brisbane, QLD, 4000, Australia
[e] Centre for Biomedical Technology, Queensland University of Technology (QUT), Brisbane, QLD, 4000, Australia
[f] Griffith Institute for Drug Discovery (GRIDD), Griffith University, Brisbane, QLD, 4111, Australia
[g] Menzies Health Institute Queensland (MIHQ), Griffith University, Brisbane, QLD, 4111, Australia

ARTICLE INFO

Keywords:
SARS-CoV-2
Paper based sensor
Colorimetric assay
Biothiol

ABSTRACT

Severe acute respiratory syndrome coronavirus 2 (SARS-CoV-2) is a serious threat to human health. Current methods such as reverse transcription polymerase chain reaction (qRT-PCR) are complex, expensive, and time-consuming. Rapid, and simple screening methods for the detection of SARS-CoV-2 are critically required to fight the current pandemic. In this work we present a proof of concept for, a simple optical sensing method for the screening of SARS-CoV-2 through its spike protein subunit S1. The method utilizes a target-specific extractor chip to bind the protein from the biological specimens. The disulfide bonds of the protein are then reduced into a biothiol with sulfhydryl (SH) groups that react with a blue-colored benzothiazole azo dye-Hg complex (BAN-Hg) and causes the spontaneous change of its blue color to pink which is observable by the naked eye. A linear relationship between the intensity of the pink color and the logarithm of reduced S1 protein concentration was found within the working range 130 ng.mL^{-1}-1.3 pg mL^{-1}. The lowest limit of detection (LOD) of the assay was 130 fg mL^{-1}. A paper based optical sensor was fabricated by loading the BAN-Hg sensor onto filter paper and used to screen the S1 protein in spiked saliva and patients' nasopharyngeal swabs. The results obtained by the paper sensor corroborated with those obtained by qRT-PCR. The new paper-based sensing method can be extended to the screening of many viruses (e.g. the human immunodeficiency virus, the human polyomavirus, the human papilloma virus, the adeno associated viruses, the enteroviruses) through the cysteine residues of their capsid proteins. The new method has strong potential for screening viruses at pathology labs and in remote areas that lacks advanced scientific infrastructure. Further clinical studies are warranted to validate the new sensing method.

1. Introduction

Since the emergence of SARS-CoV-2 disease in late 2019, it has caused significant health, psychological, social, and economic side effects to millions of people [1–3]. The SARS-CoV-2 epidemic has highlighted the demand for selective, sensitive, rapid, easy-to-use, screening tools for the diagnosis of the viral infection in patients and monitoring its spread within the community [4,5].

The gold standard for the diagnosis of SARS-CoV-2 infections is the qRT-PCR test that identifies the virus genetic material in nasopharyngeal swabs [6–9]. However, this method is time-consuming, expensive and requires well-trained technicians, sophisticated lab-based equipment [10–12]. Furthermore, rigorous qRT-PCR might miss a significant portion of SARS-CoV-2 infections because of difficulties in distinguishing the optimal time for sensitive analysis in asymptomatic persons [6, 12]. Several other screening methods such as loop-mediated isothermal

* Corresponding author. School of Chemistry and Physics, Faculty of Science, Queensland University of Technology (QUT), Brisbane, QLD, 4000, Australia.
E-mail address: e.kiriakous@qut.edu.au (E.L. Izake).

https://doi.org/10.1016/j.talanta.2022.123630
Received 26 April 2022; Accepted 29 May 2022
Available online 31 May 2022

amplification (LAMP), clustered regularly interspaced short palindromic repeats (CRISPR), recombinase polymerase amplification (RPA), immunoassays, and biosensors have been presented as quick point-of-care (POC) tools for the diagnosis of SARS-CoV-2 infection [13–18]. Among the biosensing platforms, POC devices that use Lateral flow assays (LFAs) for antigen detection were demonstrated for the rapid screening at home and in clinics. Despite being rapid, the LFA-based screening kits are usually of lower sensitivity and specificity when compared to the qRT-PCR test [19,20]. Methods based on surface-enhanced Raman Spectroscopy (SERS), field-effect transistor (FET), electroluminescence, localized surface plasmon resonance (LSPR) and electrochemical sensing have been demonstrated in the literature [21–27]. Despite the high sensitivity of these methods, their complexity, high cost, and low reproducibility, hinder their translation to POC use. Colorimetric assays have been utilized to detect SARS-CoV-2 in wastewater and saliva [28]. Antibody-coated gold nanoparticles (mAb @ AuNPs) were also developed for the detection of the SARS-CoV-2 in saliva by UV–Visible spectroscopy. However, the low sensitivity of the method (LOD = 48 ng mL^{-1}) and the potential non-specific aggregation of the AuNPs in the presence of cysteine amino acid and/or other thiol compounds in the saliva matrix makes it unreliable for practical POC applications [29,30]. Therefore, new sensitive, selective, rapid, cost-effective, easy-to-use, sensors and analytical tools are still highly required and have huge demand from the public health sector.

SARS-CoV-2 is a member of the coronavirus family, that has a crown-like layer of spike protein that surrounds the central, spherical portion of the virus [31]. The spike protein consists of S1 and S2 subunits that mediate the viral fusion and entry into host epithelial cells lining mucosal surfaces such as the lungs. The S1 and S2 proteins have many cysteine residues in their molecular structures that are interconnected through disulfide bonds [32–37]. The S1 protein has been considered as a prime target for many screening tests for the virus [38–41].

In this work, we demonstrate a proof of concept for a new highly specific, simple paper-based optical sensor for the colorimetric detection of SARS-CoV-2 through its S1 protein structure. Target-specific extractor chip was fabricated by attaching anti S1 monoclonal antibody fragments onto the surface of gold-coated silicon nanopillar chip. The extractor chip was utilized for selectively binding and purification of the S1 protein from an aqueous protein mixture and spiked saliva. The purified S1 protein was converted into a biothiol by a simple reduction process of its disulfide bond structure in 10 min modified. The free SH functional groups of the produced biothiol react spontaneously with our reported blue colored benzothiazole azo dye-Hg complex (BAN-Hg) [42,43], to cause its dissociation and the change of its blue color to pink which clearly can be seen by the naked eye and UV–Visible down to 130 fg mL^{-1}. To develop a paper-based sensor for SARS-CoV-2 at POC, the BAN-Hg sensor was loaded onto filter paper discs and used to screen the S1 protein in nasopharyngeal swabs from COVID-19 patients within 40 min. A schematic illustration of the working principles within the new SARS-CoV-2 optical sensing method is depicted in Scheme 1.

2. Materials and methods

2.1. Chemicals and reagents

Hydrochloric acid (HCl), mercury nitrate (II) monohydrate, sodium hydroxide, phenylalanine, 1-buthanthiol, glycine, human insulin, L-cysteine, phosphate-buffered saline (PBS), acetonitrile, cardiac troponin I (cTnI), 1-ethyl-3-(3-dimethylaminopropyl) carbodiimide (EDC) and N-hydroxysuccinimide (NHS) were purchased from Sigma-Aldrich (USA). Recombinant SARS-CoV-2 S1 protein was purchased from GenScript Biotech (Singapore). Monoclonal mouse anti S1 antibody was obtained from Sino Biological, Inc (China). Immobilized Tris [2-carboxyethyl] phosphine hydrochloride gel (TCEP gel) was obtained from Thermo Fisher Scientific (Australia). Tumor necrosis factor-alpha (TNF-α) and human recombinant erythropoietin (EPO) were obtained from Abcam (Australia). Protein LoBind tubes were obtained from Eppendorf (Australia). Illustra NAP-5 47 pre-packed disposable columns were obtained from Life Science GE Healthcare (Australia). Gold-coated silicon nanopillar substrates (Au@SNP) were obtained from Silmeco ApS (Denmark). Gold-coated copper oxide (Au@CuO) disc from protophysics (Australia, https://protophysics.com.au/product/bcupv/).

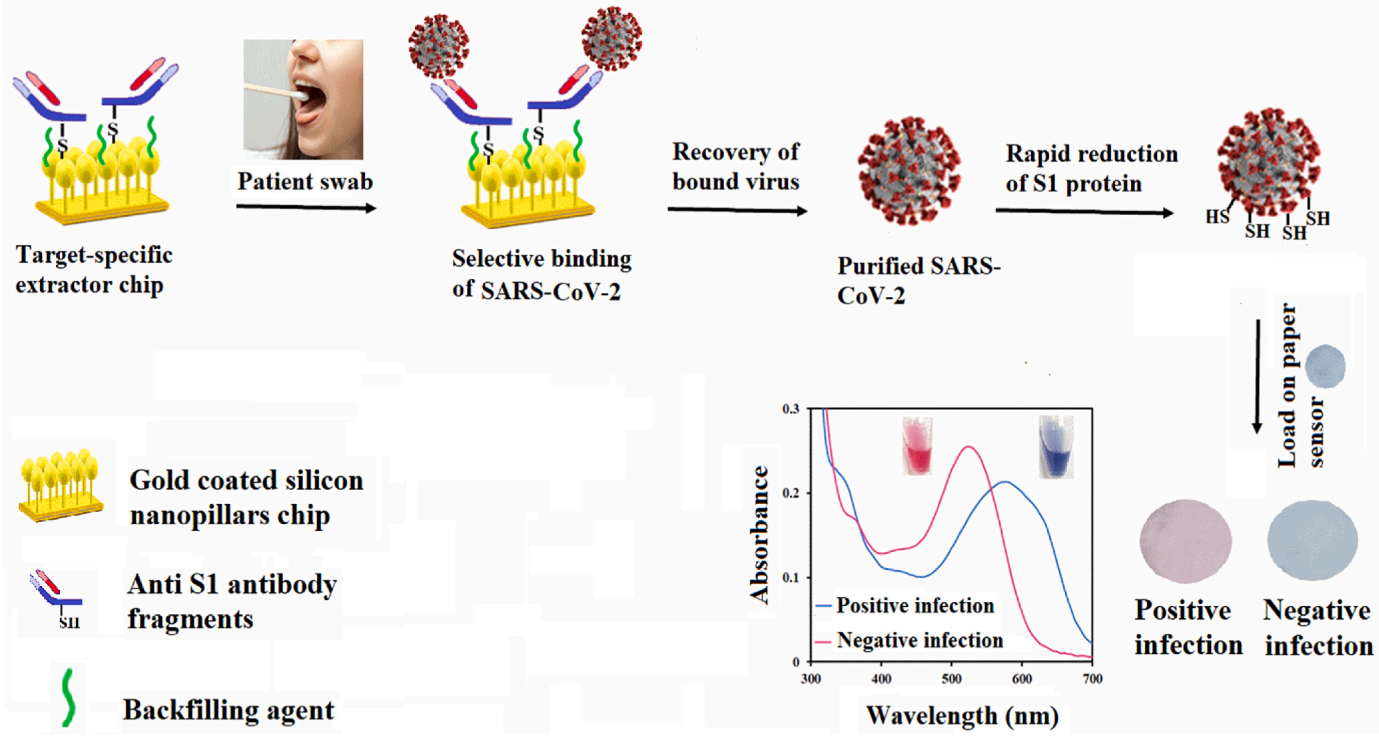

Scheme 1. Schematic illustration of selective binding and paper based colorimetric sensor for SARS-CoV-2 detection through its S1 protein.

Deionized water was used to prepare the aqueous solutions.

Saliva samples were self-donated by one of the authors (Kristyan Guppy-Coles). The use of human saliva samples and nasopharyngeal swabs was approved by the Human Research Ethics committee of the Royal Brisbane Women hospital (RBWH) (HREC/2021/QRBW/70209), and administratively by QUT Human Research Ethics committee (approval numbers, 1,900,000,820, 2,000,001,115). Patient nasopharyngeal swabs from Sullivan Nicolaides Pathology were screened at their PC2 lab (Bowen Hill, Brisbane, Australia) under the ethical approvals from RBWH and QUT (approval numbers HREC/2021/QRBW/70209, 2,000,001,115 respectively) and under QUT biosafety approval number 3891–1457.

2.2. Instrumentation

A Varian Cary 60 spectrophotometer (wavelength range 200–800 nm) was used for the UV–Visible measurements. SERS spectra were measured using a handheld Raman spectrometer in the raster orbital scanning mode with a spectral resolution of 12 cm^{-1} and wavelength ranging from 400 to 1800 cm^{-1} (Ocean Optics, USA). A laser beam at 785 nm was used to probe the sample. The laser power at the sample was set at 5 mW. Each measurement was carried out using 5 accumulations for a total acquisition time of 1 s. The fluorescence and background noise in the acquired spectra were corrected automatically using the algorithm software of the instrument (OceanView Spectroscopy 1.5.07).

2.3. Preparation of BAN-Hg complex stock solution

A 1×10^{-4} M of the benzothiazole azo dye (BAN) was prepared in ACN: H_2O solvent (1:1 v/v) according to the method described by Gholami et al. [42]. A 5×10^{-5} M stock solution of the blue colored BAN-Hg complex was prepared by mixing the BAN solution (1000 μL) with Hg (II) solution (500 μL, 1×10^{-4} M) and adjusting the pH of the mixture to 8 [42].

2.4. Preparation of S1 protein standard solution

A stock solution of 2.01 mg mL^{-1} was used to prepare different concentrations of the protein (780 $ng.mL^{-1}$- 780 fg mL^{-1}) by serial dilution using 1 × PBS (pH = 7.4).

2.5. Rapid reduction of the S1 protein and determination by BAN-Hg sensor

Immobilized TCEP gel (100 μL) was added to S1 protein solution (100 μL, 780 ng mL^{-1}) and the mixture vortexed thoroughly and incubated at room temperature (r.t) for 10 min, to ensure the complete reduction of disulfide bonds of the protein. To remove immobilized TCEP gel and recover reduced protein, it was centrifuged at 1000 rpm for 1 min 100 μL of the reduced S1 protein solution was transferred into a clean LoBind tube. BAN-Hg complex (200 μL, 45.16 μg mL^{-1}) was added to the reduced S1 protein solution and the absorbance of the developed pink color was measured using UV–Visible spectroscopy.

2.6. Effect on time the reaction between reduced S1 protein and BAN-Hg sensor

Unreduced S1protein (100 μL, 7.8 ng mL^{-1}) was mixed with TCEP gel (100 μL) in a LoBind tube, vortexed and kept for 10 min (r.t). The TCEP gel was removed from the solution by centrifuge at 1000 rpm for 1 min 100 μL of the reduced S1 protein solution was transferred into a clean LoBind tube and mixed with BAN-Hg sensor (200 μL, 45.16 μg mL^{-1}). UV–Visible measurements were carried out to record the absorbance of the developing, pink-colored solution at 530 nm. The measurements were carried out between zero and 5 min from adding the BAN-Hg sensor.

2.7. Quantification of reduced S1 protein by UV–Visible

100 μL of S1 protein solutions in the concentration range 780 ng mL^{-1} - 780 fg mL^{-1} were mixed thoroughly with 100 μL of TCEP gel and incubated for 10min (r.t). The TCEP gel was removed from the solution by centrifuging at 1000 rpm for 1 min 100 μL aliquots of the reduced S1 protein solutions were transferred into clean LoBind tubes and mixed with BAN-Hg sensor (200 μL, 45.16 μg mL^{-1}). UV–Visible measurements were carried out to measure the absorbance of the developing, pink-colored solution at 530 nm (n = 5).

2.8. Fabrication of target-specific extractor chip for S1 protein

30 μL of TCEP neutral solution (40 Mm) were mixed with 30 μL of anti- S1antibody (2×10^{-7} M), vortexed for 3 min and incubated for 10 min (r.t) to produce antibody fragments through reduction of the hinge-region disulfide bonds of the antibody [43]. An Au@SNP substrate was immersed into the TCEP/antibody fragments mixture and incubated at 4 °C overnight to allow to attach antibody fragments onto the surface of the chip through the formation of gold-sulfur bonds. The attachment of the antibody fragments to the Au@SNP substrate was confirmed by SERS measurement (Fig. S1). Then the chip was washed 5 times with 1 × PBS (100 μL, pH = 7.4) to remove any unbound and physically adsorbed antibodies. The chip was immersed in 3-mercaptopropionic acid (100 μL, 1×10^{-8} M) for 1 h at 4 °C to block the remaining area on the bare Au surface of the chip. Finally, the excess of 3-mercaptopropionic acid was removed by rinsing the chip 5 times with 1 × PBS (100 μL, pH = 7.4). The fabricated extractor chip was then suspended in 1 × PBS (100 μL) and kept at 4 °C for future use.

2.9. Fabrication of paper-based optical sensor for screening of S 1 protein

600 μL of 45.16 μg mL^{-1} BAN-Hg complex in ACN: H_2O (1:1, v/v) were prepared according to the method described by Gholami et al. [42]. Filter paper discs were immersed in the BAN-Hg sensor for a few minutes then air-dried. The paper sensors were stored at room temperature for future use.

2.10. Control tests

To confirm the specificity of the antibody-coated extractor chip, a negative control sample was prepared by mixing equal volumes of 10 ng mL^{-1} stock solutions of L-cysteine, phenylalanine, insulin, EPO, cTnI and TNF-α and diluting the mixture with 1 × PBS (pH = 7.4) to the final concentration of 1 ng mL^{-1} of each amino acid and protein. To prepare a positive control sample, equal volumes of 7.8 ng mL^{-1} solutions of S 1 protein, L-cysteine, phenylalanine, insulin, EPO, cTnI and TNF-α were mixed and diluted with 1 × PBS (pH = 7.4) to the final concentration of 0.78 ng mL^{-1} of each amino acid and protein. Target-specific extractor chips were added to 100 μL of the positive and negative control samples in LoBind tubes and kept for 20 min (r.t) to bind the target protein. The chips were then removed, rinsed 5 times with 1 × PBS (100 μL, pH = 7.4) to wash any physically adsorbed interfering biomolecules.

To release the bound protein from the chips, they were incubated in glycine- HCl buffer (100 μL, pH = 2.5) for 5 min (r.t) [43–45]. The glycine buffer was then removed by loading the extract solution onto a size exclusion column (SEC). After passing the buffer, the trapped protein was eluted from the column using 1 × PBS (400 μL, pH = 7.4), 100 μL of the purified and eluted protein (from the positive and negative control samples) were mixed with TCEP gel (100 μL) in LoBind tubes and kept for 10 min (r.t). The TCEP gel was removed by centrifuging the solutions at 1000 rpm for 1 min 100 μL aliquots of the reduced protein solution were transferred into clean LoBind tubes, mixed with BAN-Hg sensor (200 μL, 45.16 μg mL^{-1}) and the mixtures were screened by UV–Visible spectroscopy (n = 5).

2.11. Selective binding and screening of S1 protein from spiked saliva

10 μL of S1 protein solution (7.8 ng mL^{-1} in 1 × PBS) was spiked into 100 μL of human saliva to the final concentration of 0.78 ng mL^{-1}. A fabricated extractor chip was added to 100 μL of the spiked saliva in a LoBind tube and incubated for 20 min (r.t) to bind the S1 protein. The chip was then removed, rinsed 5 times with 1 × PBS (100 μL, pH = 7.4) to wash out the weakly adsorbed interfering biomolecules. The bound S1 protein was released from the chip, by incubation in glycine buffer (100 μL, pH = 2.5) for 5 min (r.t) [42–44]. The glycine buffer was then removed from the pure protein by loading the solution onto a SEC and eluting with 1 × PBS eluent (400 μL, pH = 7.4). 100 μL of the eluted purified protein solutions were mixed with TCEP gel (100 μL) and kept for 10 min (r.t). The TCEP gel was removed by centrifuging the solution at 1000 rpm for 1 min 100 μL of the reduced protein was transferred into a clean LoBind tube, mixed with BAN-Hg sensor (200 μL, 45.16 μg mL^{-1}) and screened by UV–Visible (n = 5). The reduced protein was also monitored by the paper-based optical sensor. 15 μL of the reduced protein was loaded onto the paper sensor and the color change from blue to pink was monitored by the naked eye. For comparison, a blank saliva sample (not spiked with S1 protein) was processed using the above procedures and the reduced extract screened by UV–Visible (n = 5), and paper-based optical sensor as described above.

2.12. Selective binding and screening of S1 protein in patient nasopharyngeal swabs

Swabs from a healthy individual and a COVID-19 patient, were provided by Sullivan Nicolaides Pathology lab. The swabs were screened by the pathology lab using RT-qPCR. To rescreen the nasopharyngeal swabs by our new optical sensing method, the swabs were resuspended in a viral transport medium (VTM) (pH = 7.4). 20 μL of the VTM solutions were mixed with 1 × PBS (80 μL, pH = 7.4) and vortexed for 1 min 100 μL of the mixture was incubated with a prepared target-specific extractor chip in a LoBind tube for 20 min in order to bind the S1 protein. The extractor chip was then transferred into a clean LoBind tube that contains glycine buffer (100 μL, pH = 2.5) to release the bound protein. The solution was then loaded onto a SEC to remove the buffer and the purified protein was collected using 1 × PBS eluent (400 μL, pH = 7.4). 100 μL of the eluted protein was mixed with TCEP gel (100 μL) and kept for 10 min (r.t). The gel was then removed by centrifuging the solution as described above and 15 μL of the reduced S1 protein was loaded onto the paper-based sensor at room temperature and the sensor color change from blue to pink was monitored by the naked eye.

3. Results and discussion

We recently demonstrated the dissociation reaction between the BAN-Hg reagent and biothiols that contain free sulfhydryl functional groups in their molecular structures [42,43]. The molecular structure of the S1 protein contains disulfide bonds between its cysteine residues Cys15-Cys136, Cys828-Cys853 and Cys840-Cys851 [36]. Therefore, the S1 protein can be chemically converted into a biothiol using TCEP reducing agent to reduce its disulfide bonds [43,44,46]. The reduced S1 protein should be able to dissociate the BAN-Hg complex due to the high affinity of sulfur to the Hg^{2+} moiety of the complex [42,43].

3.1. Reaction of the BAN-Hg sensor with unreduced and reduced S1 protein

As shown in Fig. 1, the BAN-Hg sensor did not react with the unreduced S1 protein and its color and UV–Visible absorbance at 585 nm did not change (Fig. 1B). By contrast, the blue color of the BAN-Hg sensor changed to pink when it was reacted with the reduced S1 protein, and its UV–Visible absorption band shifted to 530 nm (55 nm redshift) (Fig. 1C) due to the dissociation of the dye-Hg complex and the release of BAN dye in the solution [47]. This result represents a proof of concept that the BAN-Hg sensor interacts only with the free SH groups that form when the disulfide bonds between the cysteine residues are reduced.

3.2. Time effect on the reaction between BAN-Hg sensor and reduced S1 protein

The reaction between reduced S1 protein and the BAN-Hg sensor was investigated by UV–Visible spectroscopy at different time intervals. As shown by Fig. 2, the color change of the sensor from blue to pink was immediate upon the reduced S1 protein addition and the intensity of the UV–Visible absorption band of the BAN dye at 530 nm did not change after 5 min of addition (Fig. S2).

3.3. Sensitivity of the BAN-Hg sensor towards reduced S1 protein

A good linear relationship was found between the intensity of absorption band at 530 nm and log concentration of the reduced S1 protein in a working range between 130 ng mL^{-1} and 130 fg mL^{-1} and presented by the regression equation y = 0.0037x + 0.2832 (R^2 = 0.98) (Fig. 2A and B and S3). As indicated by Fig. 2A and S3, the LOD of the colorimetric detection of reduced S1 protein was 130 fg mL^{-1} which is sensitive enough to detect SARS-CoV-2 S1 protein in real life samples [48–50]. Therefore, the BAN-Hg sensor can be utilized as a sensor for the diagnosis of COVID-19 infections through the detection of trace amounts of the SARS-CoV-2 S1 protein.

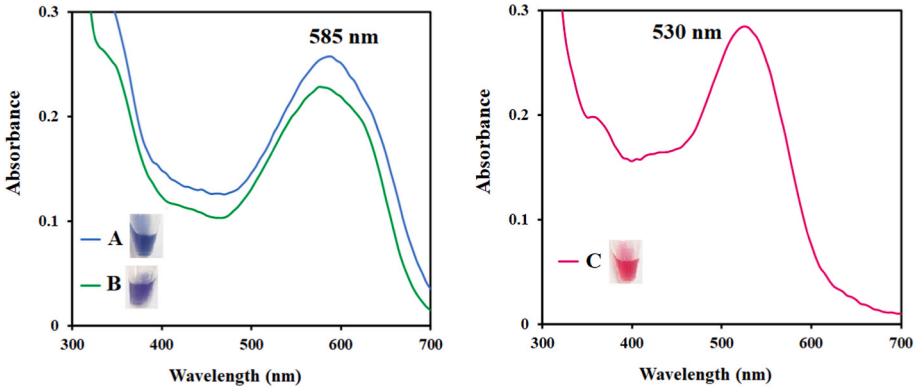

Fig. 1. **(A)** UV–Visible spectra of the BAN-Hg sensor, **(B)** UV–Visible spectra of the BAN-Hg sensor after mixing with unreduced S1 protein (390 ng mL^{-1}), **(C)** UV–Visible spectra of the BAN-Hg sensor after mixing with reduced S1 protein (390 ng mL^{-1}).

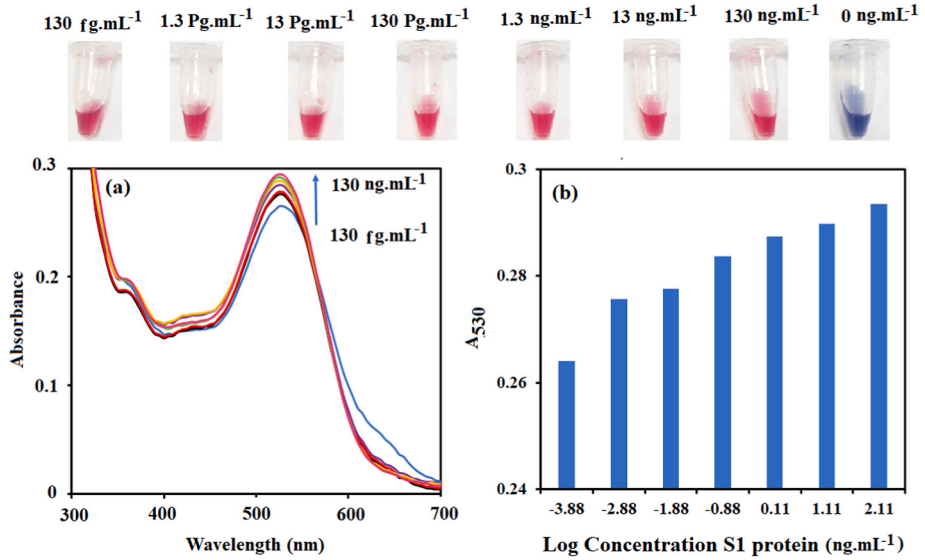

Fig. 2. **(A)** UV–Visible spectra of the BAN-Hg sensor upon addition of various concentrations of the reduced S1 protein (130 ng.mL^{-1}- 130 fg mL^{-1}), **(B)** Plot of the intensity of the absorption band at 530 nm versus log concentration of reduced S1 protein (130 ng mL^{-1} to 130 fg mL^{-1}).

3.4. Paper-based sensor for the detection of the SARS-CoV-2 spike protein (S1)

In recent years, paper-based sensors have attracted strong attention for real-life applications in many areas such as environmental monitoring, food safety, drug analysis, and molecular diagnostics [51–54]. The paper-based sensors offer the advantages of low cost, simplicity, ease of disposal, and environmental friendliness [55–57]. Therefore, we aimed to develop a paper-based sensor for the ultra-trace detection of the S1 protein in SARS-CoV-2 patients. For this purpose, The BAN-Hg sensor was loaded onto the filter paper discs and utilized for the screening of the reduced S1 protein solutions (Fig. 3). As indicated, the blue-colored paper sensor spontaneously turned to pink upon addition of different concentrations of the reduced S1 protein down to 390 fg mL^{-1}.

3.5. Specific binding and detection of the S1 protein from negative and positive control and spiked saliva samples

For the specific detection of the S1 protein in biological specimens, isolation and purification of the target analyte from the complex biological matrix are necessary. Therefore, a target-specific extractor chip was synthesized through the reduction of the hinge region disulfide bonds of anti-S1 protein antibody in order to generate thiol-ended antibody fragments. The antibody fragments were chemisorbed onto an Au@SNP chip, forming Au–S bonds [43]. The antibody fragment attachment to the chip surface was confirmed by SERS. As indicated by Fig. S1, diagnostic Raman bands of IgG molecules were observed on the chip after the chemisorption of the Fab 2 fragments (Table S1). To avoid the non-specific binding of interfering molecules from the biological matrix, the unoccupied sites on the surface of the functionalized chip were backfilled with 3-mercaptopropionic acid [44,45].

The fabricated extractor chip was used to bind the S1 protein from negative and positive control samples. The bound protein was recovered by lowering the pH of the chip using the glycine buffer solution (pH = 2.5). The recovered protein was purified from the glycine buffer using SEC and reduced by TCEP to convert it into a biothiol that reacts with the BAN-Hg sensor in solution and on the paper senor. As indicated by Fig. 4A, the extract solution from the negative control sample did not cause any change to the absorption spectra and color of the BAN-Hg sensor, thus confirming the absence of any biothiol in the extract. By contrast, the extract solution from the positive control sample caused a spontaneous color change to the absorption spectra and color of the BAN-Hg sensor (Fig. 4B). Similar results were obtained from the unspiked and spiked saliva samples (Fig. 4C and D). These results demonstrate a proof of concept on the specificity of the target-specific extractor chip to selectively bind the S1viral protein over other proteins in the sample. The specificity of the extractor chip is attributed to the high affinity of the S1 antibody towards the target protein as indicated by the antibody affinity data [https://www.sinobiological.com/antibodies/cov-spike-40592-mm57].

The paper-based optical sensor showed a significant color change from blue to pink for the positive sample (Fig. 4B). The target-specific extractor was also utilized to selectively bind the S1 protein from blank and spiked human saliva samples. The purification and reduction processes were carried out as indicated earlier. The purified and reduced protein extract, from the blank and spiked saliva samples, was reacted with the BAN-Hg sensor in solution and on the paper senor. As shown in Fig. 4C, there was no change in the color of the BAN-Hg sensor when it was reacted with the extract solution from the blank saliva sample. On the contrary, the extract solution from the spiked saliva sample caused changes in the absorption spectra and color of the BAN-Hg sensor (Fig. 4D), thus confirming the binding of the S1 protein and its conversion to biothiol through the reduction process. These results provide

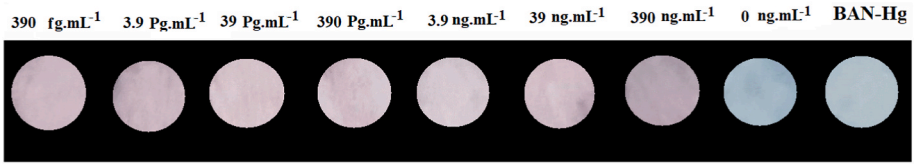

Fig. 3. The color change of the paper-based optical sensor in the presence of trace concentrations of the reduced S1 protein (390 ng.mL^{-1}- 390 fg mL^{-1}). (For interpretation of the references to color in this figure legend, the reader is referred to the Web version of this article.)

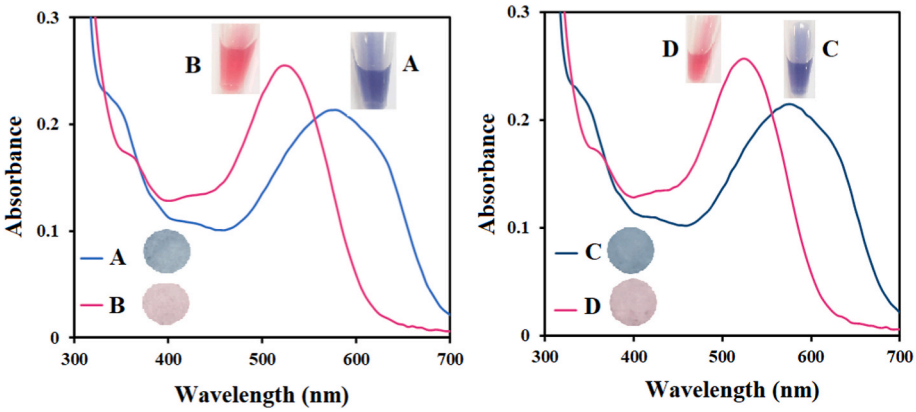

Fig. 4. Change in UV–Visible spectra and the color of the BAN-Hg solution and paper sensor after reaction with **(A)** a negative control sample and, **(B)** a positive control sample (spiked with S1 protein), **(C)** blank saliva, **(D)** saliva spiked with S1 protein. (For interpretation of the references to color in this figure legend, the reader is referred to the Web version of this article.)

a proof of concept on the potential of the target-specific extractor chip and optical sensor for screening the S1 protein in biological specimens.

3.6. Detection of the S1 protein in nasopharyngeal swabs from SARS-CoV-2 patients

To demonstrate the paper-based optical sensor for the diagnosis of SARS-CoV-2 infection, it was used to re-screen nasopharyngeal swabs from a healthy individual and a COVID-19 patient who have been screened by Sullivan Nicolaides pathology lab using qRT-PCR method. The RNA of the SARS-CoV-2 virus was not detected in the swab from the healthy person (e Gene Count = 0) while the swab from the infected person showed the presence of the RNA of the virus (e Gene Count = 20.58, N2 Gene Count = 20.8). The swabs were resuspended in full in VTM and the solutions were incubated with target-specific extractor chips to bind the S1 protein in the sample. The purified and reduced protein from the swabs was loaded onto paper-based optical sensors and the color change was monitored by the naked eye. As indicated by Fig. 5, the sample from the healthy individual did not cause any color change to the optical sensor while the sample from the infected person caused a spontaneous color change from blue to pink, thus confirming the presence of the S1 protein of the SARS-CoV-2 virus in the sample.

The qRT-PCR results agreed with those obtained by the paper-based optical sensor, thus providing proof of concept on its potential for the screening of SARS-CoV-2 at POC and in clinical settings. These results warrant a large clinical trial to validate the new sensing method.

To reduce the cost of the new assay, we attempted to fabricate S1 target-specific extractor chip using an inexpensive Au@CuO disc instead of Au@SNP. The fabrication procedure was applied to the Au@CuO substrate. As indicated by Fig. S4, the anti-S1 antibody molecules were attached to the disc surface and the target-specific chip was successfully synthesized. The cost of the Au@CuO disc is 2.5$. Therefore, by using this material and the disposable paper-based optical sensor, the overall cost of the new assay for SARS-CoV-2 is significantly lower than that of the qRT-PCR assay.

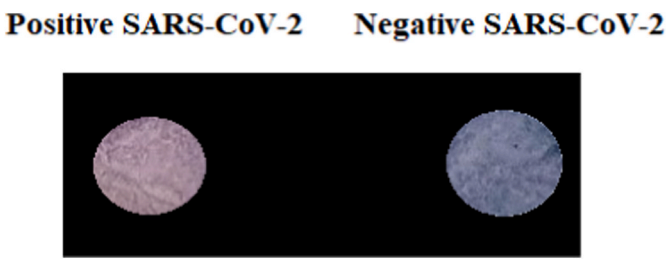

Fig. 5. Color change of the paper-based optical sensor after interaction with nasal swab samples from healthy and infected persons. (For interpretation of the references to color in this figure legend, the reader is referred to the Web version of this article.)

Other sensors have been recently developed and demonstrated for the screening of SARS-CoV-2 infection in patients (Table S2). However, many of these methods require the use of sophisticated sensing schemes and materials that makes the proposed test expensive, not suitable for POC setting, or require advanced scientific equipment. By contrast, the new paper-based sensor is easy to fabricate and uses the naked eye as a detector to monitor the color change caused by the S1 protein of the SARS-CoV-2 virus. In addition, sensitivity of the BAN-Hg sensor is satisfactory for the screening of the S1 protein in biological specimens at points of care.

4. Conclusions

A new target-specific extractor chip and paper-based optical sensor were synthesized and used to provide a proof of concept on the colorimetric detection of the S1 protein by UV–Visible and the naked eye in biological specimens. The new paper-based optical sensor has high sensitivity (LOD = 130 fg mL^{-1}) and a fast response towards the S1 protein of the SARS-CoV-2 virus. Therefore, the new sensor was utilized for the screening of S1 protein in aqueous media, and spiked human saliva. The color change of the optical sensor from blue to pink was easily observable by the naked eye. Therefore, the new sensor was used to screen patient nasopharyngeal swabs. The results agreed with those acquired by qRT-PCR test. The low cost, simplicity and fast response of the new paper-based optical sensor underpins its potential for the screening of SARS-CoV-2 infections at POC and in clinical settings. The authors are currently organizing a clinical trial to screen many patient samples and fully validate the new sensing method.

Credit author statement

Mahnaz.D.Gholami prepared the new sensor, carried out the experimental work, collected and analysed experimental data, interpreted the results, and drafted the manuscript. **Kristyan Guppy-Coles** carried out tests at pathology labs on patient samples and collected experimental data, compared them to PCR results. **Serena Nihal** prepared extractor materials. **Daman Langguth** gave access to patient samples, contributed to the scientific discussion on the criteria and optimization of the new sensor. **Prashant Sonar** contributed to the design, synthesis of the new sensor. **Godwin A. Ayoko** guided the analytical procedures to validate the new sensor. **Chamindie Punyadeera** guided the work on the saliva matrix and contributed to the discussion of the obtained results. **Emad L. Izake** conceived the

scientific concepts for the new sensing approach, contributed to the design of the experimental work, contributed to the interpretation of the experimental data, contributed to the writing, and editing of the article manuscript.

Declaration of competing interest

The authors declare that they have no known competing financial interests or personal relationships that could have appeared to influence the work reported in this paper.

Acknowledgment

The authors would like to acknowledge the support from Faculty of Science for the access to Central Analytical Research Facility (CARF). The authors would like to thank Dr Jenny Robson, Dr Sarah Cherian, Dr Carl Kennedy, Mr Shane Byrne, Mr Peter Hobson, Ms Tammie Hunt and Ms Danielle Thygesen from Sullivan Nicolaides Pathology lab for their support to this work.

Appendix A. Supplementary data

Supplementary data to this article can be found online at https://doi.org/10.1016/j.talanta.2022.123630.

References

[1] A.S. Arshad, M. Baloch, N. Ahmed, A.A. Arshad, A. Iqbal, The outbreak of Coronavirus Disease 2019 (COVID-19)-An emerging global health threat, J. Infect. Public Health. 13 (2020) 644–646, https://doi.org/10.1016/j.jiph.2020.02.033.
[2] B. Hu, H. Guo, P. Zhou, Z.L. Shi, Characteristics of SARS-CoV-2 and COVID-19, Nat. Rev. Microbiol. 19 (2021) 141–154, https://doi.org/10.1038/s41579-020-00459-7.
[3] B. Kotlar, E. Gerson, S. Petrillo, A. Langer, H. Tiemeier, The impact of the COVID-19 pandemic on maternal and perinatal health: a scoping review, Reprod. Health 18 (2021) 10, https://doi.org/10.1186/s12978-021-01070-6.
[4] A. Fernandez-Montero, J. Argemi, J.A. Rodríguez, A.H. Ariño, L. Moreno-Galarraga, Validation of a rapid antigen test as a screening tool for SARS-CoV-2 infection in asymptomatic populations. Sensitivity, specificity and predictive values, EClinicalMedicine 37 (2021), 100954, https://doi.org/10.1016/j.eclinm.2021.100954.
[5] L.E. Brümmer, S. Katzenschlager, M. Gaeddert, C. Erdmann, S. Schmitz, M. Bota, M. Grilli, J. Larmann, M.A. Weigand, N.R. Pollock, A. Macé, S.S. Carmona, Ongarello, J.A. Sacks, C.M. Denkinger, Accuracy of novel antigen rapid diagnostics for SARS-CoV-2: a living systematic review and meta-analysis, PLoS Med. 18 (2021), e1003735, https://doi.org/10.1371/journal.pmed.1003735.
[6] Z. Zhang, Q. Bi, S. Fang, L. Wei, X. Wang, J. He, Y. Wu, X. Liu, W. Gao, R. Zhang, W. Gong, Q. Su, A.S. Azman, J. Lessler, X. Zou, Insight into the practical performance of RT-PCR testing for SARS-CoV-2 using serological data: a cohort study, Lancet Microbe 2 (2021) e79–e87, https://doi.org/10.1016/S2666-5247(20)30200-7.
[7] O. Vandenberg, D. Martiny, O. Rochas, A. Belkum, Z. Kozlakidis, Considerations for diagnostic COVID-19 tests, Nat. Rev. Microbiol. 19 (2021) 171–183, https://doi.org/10.1038/s41579-020-00461-z.
[8] C. Aranha, V. Patel, V. Bhor, D. Gogoi, Cycle threshold values in RT-PCR to determine dynamics of SARS-CoV-2 viral load: an approach to reduce the isolation period for COVID-19 patients, J. Med. Virol. 93 (2021) 6794–6797, https://doi.org/10.1002/jmv.27206.
[9] A. Banko, G. Petrovic, D. Miljanovic, A. Loncar, M. Vukcevic, D. Despot, A. Cirkovic, Comparison and sensitivity evaluation of three different commercial real-time quantitative PCR kits for SARS-CoV-2 detection, Viruses 13 (2021) 1321, https://doi.org/10.3390/v13071321.
[10] S. Sethi, T. Chakraborty, Molecular (real-time reverse transcription polymerase chain reaction) diagnosis of SARS-CoV-2 infections: complexity and challenges, J. Lab. Med. 45 (2021) 135–142, https://doi.org/10.1515/labmed-2020-0135.
[11] A. Tahamtan, A. Ardebili, Real-time RT-PCR in COVID-19 detection: issues affecting the results, Expert Rev. Mol. Diagn 20 (2020) 453–454, https://doi.org/10.1080/14737159.2020.1757437.
[12] S.A. Bustin, T. Nolan, RT-qPCR testing of SARS-CoV-2: a primer, Int. J. Mol. Sci. 21 (2020) 3004, https://doi.org/10.3390/ijms21083004.
[13] J. Moon, H.J. Kwon, D. Yong, I.C. Lee, H. Kim, H. Kang, E.K. Lim, K.S. Lee, J. Jung, H.G. Park, T. Kang, Colorimetric detection of SARS-CoV-2 and drug-resistant pH1N1 using CRISPR/dCas9, ACS Sens. 5 (2020) 4017–4026, https://doi.org/10.1021/acssensors.0c01929.
[14] R. Augustine, A. Hasan, S. Das, R. Ahmed, Y. Mori, T. Notomi, B.D. Kevadiya, A. S. Thakor, Loop-mediated isothermal amplification (LAMP): a rapid, sensitive, specific, and cost-effective point-of-care test for coronaviruses in the context of COVID-19 pandemic, Biology 9 (2020) 182, https://doi.org/10.3390/biology9080182.
[15] Y.L. Lau, Ib Ismail, N.Ib Mustapa, M.Y. Lai, T.S. Tuan Soh, A. Haji Hassan, K. M. Peariasamy, Y.L. Lee, M.K.B. Abdul Kahar, J. Chong, P.P. Goh, Development of a reverse transcription recombinase polymerase amplification assay for rapid and direct visual detection of Severe Acute Respiratory Syndrome Coronavirus 2 (SARS-CoV-2), PLoS One 16 (2021), e0245164, https://doi.org/10.1371/journal.pone.0245164.
[16] N. Adnan, S.S. Khandker, A. Haq, M.A. Chaity, A. Khalek, A.Q. Nazim, T. Kaitsuka, K. Tomizawa, M. Mie, E. Kobatake, M. Haque, M.R. Jamiruddin, Detection of SARS-CoV-2 by antigen ELISA test is highly swayed by viral load and sample storage condition, Expert Rev. Anti Infect. Ther. 20 (2021) 473–481, https://doi.org/10.1080/14787210.2021.1976144.
[17] B.D. Kevadiya, J. Machhi, J. Herskovitz, M.D. Oleynikov, W.R. Blomberg, N. Bajwa, D. Soni, S. Das, M. Hasan, M. Patel, A.M. Senan, S. Gorantla, J. McMillan, B. Edagwa, R. Eisenberg, C.B. Gurumurthy, S.P.M. Reid, C. Punyadeera, L. Chang, H.E. Gendelman, Diagnostics for SARS-CoV-2 infections, Nat. Mater. 20 (2021) 593–605, https://doi.org/10.1038/s41563-020-00906-z.
[18] A. Eftekhari, M. Alipour, L. Chodari, S. Maleki Dizaj, M. Ardalan, M. Samiei, S. Sharifi, S. Zununi Vahed, I. Huseynova, R. Khalilov, E. Ahmadian, M. A. Cucchiarini, Comprehensive review of detection methods for SARS-CoV-2, Microorganisms 9 (2021) 232, https://doi.org/10.3390/microorganisms9020232.
[19] B.D. Grant, C.E. Anderson, J.R. Williford, L.F. Alonzo, V.A. Glukhova, D.S. Boyle, B. H. Weigl, K.P. Nichols, SARS-CoV-2 coronavirus nucleocapsid antigen-detecting half-strip lateral flow assay toward the development of point of care tests using commercially available reagents, Anal. Chem. 92 (2020) 11305–11309, https://doi.org/10.1021/acs.analchem.0c01975.
[20] A. Roda, S. Cavalera, F. Di Nardo, D. Calabria, S. Rosati, P. Simoni, B. Colitti, C. Baggiani, M. Roda, L. Anfossi, Dual lateral flow optical/chemiluminescence immunosensors for the rapid detection of salivary and serum IgA in patients with COVID-19 disease, Biosens. Bioelectron. 172 (2021), 112765, https://doi.org/10.1016/j.bios.2020.112765.
[21] G. Qiu, Z. Gai, Y. Tao, J. Schmitt, G.A. Kullak-Ublick, J. Wang, Dual-functional plasmonic photothermal biosensors for highly accurate Severe acute respiratory syndrome coronavirus 2 detection, ACS Nano 14 (2020) 5268–5277, https://doi.org/10.1021/acsnano.0c02439.
[22] T. Chaibun, J. Puenpa, T. Ngamdee, N. Boonapatcharoen, P. Athamanolap, A. P. O'Mullane, S. Vongpunsawad, Y. Poovorawan, S.Y. Lee, B. Lertanantawong, Rapid electrochemical detection of coronavirus SARS-CoV-2, Nat. Commun. 12 (2021) 802, https://doi.org/10.1038/s41467-021-21121-7.
[23] A.K. Kaushik, J.S. Dhau, H. Gohel, Y.K. Mishra, B. Kateb, N.Y. Kim, D.Y. Goswami, Electrochemical SARS-CoV-2 sensing at point-of-care and artificial intelligence for intelligent COVID-19 management, ACS Appl. Bio Mater. 3 (2020) 7306–7325, https://doi.org/10.1021/acsabm.0c01004.
[24] G. Seo, G. Lee, M.J. Kim, S.H. Baek, M. Choi, K.B. Ku, C.S. Lee, S. Jun, D. Park, H. G. Kim, S.J. Kim, J.O. Lee, B.T. Kim, E.C. Park, S. Kim, Rapid detection of COVID-19 causative virus (SARS-CoV-2) in human nasopharyngeal swab specimens using field-effect transistor-based biosensor, ACS Nano 14 (2020) 5135–5142, https://doi.org/10.1021/acsnano.0c02823.
[25] M. Zhang, X. Li, J. Pan, Y. Zhang, L. Zhang, C. Wang, X. Yan, X. Liu, G. Lu, Ultrasensitive detection of SARS-CoV-2 spike protein in untreated saliva using SERS-based biosensor, Biosens. Bioelectron. 190 (2021), 113421, https://doi.org/10.1016/j.bios.2021.113421.
[26] C. Carlomagno, D. Bertazioli, A. Gualerzi, S. Picciolini, P.I. Banfi, A. Lax, E. Messina, J. Navarro, L. Bianchi, A. Caronni, F. Marenco, S. Monteleone, C. Arienti, M. Bedoni, COVID-19 salivary Raman fingerprint: innovative approach for the detection of current and past SARS-CoV-2 infections, Sci. Rep. 11 (2021) 4943, https://doi.org/10.1038/s41598-021-84565-3.
[27] C. Wang, Z. Wu, B. Liu, P. Zhang, J. Lu, J. Li, P. Zou, T. Li, Y. Fu, R. Chen, L. Zhang, Q. Fu, C. Li, Track-etched membrane microplate and smartphone immunosensing for SARS-CoV-2 neutralizing antibody, Biosens. Bioelectron. 192 (2021), 113550, https://doi.org/10.1016/j.bios.2021.113550.
[28] K. Yin, X. Ding, Z. Xu, Z. Li, X. Wang, H. Zhao, C. Otis, B. Li, C. Liu, Multiplexed colorimetric detection of SARS-CoV-2 and other pathogens in wastewater on a 3D printed integrated microfluidic chip, Sens. Actuators, B 344 (2021), 130242, https://doi.org/10.1016/j.snb.2021.130242.
[29] E. Karakuş, E. Erdemir, N. Demirbilek, L. Liv, Colorimetric and electrochemical detection of SARS-CoV-2 spike antigen with a gold nanoparticle-based biosensor, Anal. Chim. Acta 1182 (2021), 338939, https://doi.org/10.1016/j.aca.2021.338939.
[30] B.D. Ventura, M. Cennamo, A. Minopoli, R. Campanile, S.B. Censi, D. Terracciano, G. Portella, R. Velotta, Colorimetric test for fast detection of SARS-CoV-2 in nasal and throat swabs, ACS Sens. 5 (2020) 3043–3048, https://doi.org/10.1021/acssensors.0c01742.
[31] R.M. Golonka, P. Saha, B.S. Yeoh, S. Chattopadhyay, A.T. Gewirtz, B. Joe, M. Vijay-Kumar, Harnessing innate immunity to eliminate SARS-CoV-2 and ameliorate COVID-19 disease, Physiol. Genom. 52 (2020) 217–221, https://doi.org/10.1152/physiolgenomics.00033.2020.
[32] S. Hati, S. Bhattacharyya, Impact of thiol–disulfide balance on the binding of covid-19 spike protein with angiotensin-converting enzyme 2 receptor, ACS Omega 5 (2020) 16292–16298.
[33] X. Xia, Domains and functions of spike protein in SARS-cov-2 in the context of vaccine design, Viruses 13 (2021) 109, https://doi.org/10.1021/acsomega.0c02125.

[34] J. Singh, R.S. Dhindsa, V. Misra, B. Singh, SARS-CoV2 infectivity is potentially modulated by host redox status, Comput. Struct. Biotechnol. J. 18 (2020) 3705–3711, https://doi.org/10.1016/j.csbj.2020.11.016.
[35] R. Puthenveetil, C.M. Lun, R.E. Murphy, L.B. Healy, G. Vilmen, E.T. Christenson, E. O. Freed, A. Banerjee, S-acylation of SARS-CoV-2 spike protein: mechanistic dissection, in vitro reconstitution and role in viral infectivity, J. Biol. Chem. 297 (2021), 101112, https://doi.org/10.1016/j.jbc.2021.101112.
[36] Y. Cai, J. Zhang, T. Xiao, H. Peng, S.M. Sterling, R.M. Walsh Jr., S. Rawson, S. Rits-Volloch, B. Chen, Distinct conformational states of SARS-CoV-2 spike protein, Science 369 (2020) 1586–1592, https://doi.org/10.1126/science.abd4251.
[37] L. Duan, Q. Zheng, H. Zhang, Y. Niu, Y. Lou, H. Wang, The SARS-CoV-2 spike glycoprotein biosynthesis, structure, function, and antigenicity: implications for the design of spike-based vaccine immunogens, Front. Immunol. 11 (2020), 576622, https://doi.org/10.3389/fimmu.2020.576622.
[38] X. Ou, Y. Liu, X. Lei, P. Li, D. Mi, L. Ren, L. Guo, R. Guo, T. Chen, J. Hu, Z. Xiang, Z. Mu, X. Chen, J. Chen, K. Hu, Q. Jin, J. Wang, Z. Qian, Characterization of spike glycoprotein of SARS-CoV-2 on virus entry and its immune cross-reactivity with SARS-CoV, Nat. Commun. 11 (2020) 1620, https://doi.org/10.1038/s41467-020-15562-9.
[39] J. Lan, J. Ge, J. Yu, S. Shan, H. Zhou, S. Fan, Q. Zhang, X. Shi, Q. Wang, L. Zhang, X. Wang, Structure of the SARS-CoV-2 spike receptor-binding domain bound to the ACE2 receptor, Nature 581 (2020) 215–220, https://doi.org/10.1038/s41586-020-2180-5.
[40] R.M.L.C. Biancatelli, P.A. Solopov, E.R. Sharlow, J.S. Lazo, P.E. Marik, J. D. Catravas, The SARS-CoV-2 spike protein subunit S1 induces COVID-19-like acute lung injury in K18-hACE2 transgenic mice and barrier dysfunction in human endothelial cells, Am. J. Physiol. Lung Cell Mol. Physiol. 321 (2021) L477–L484, https://doi.org/10.1152/ajplung.00223.2021.
[41] Y. Wu, S. Zhao, Furin cleavage sites naturally occur in coronaviruses, Stem Cell Res. 50 (2021), 102115, https://doi.org/10.1016/j.scr.2020.102115.
[42] M.D. Gholami, S. Manzhos, P. Sonar, G.A. Ayoko, E.L. Izake, Dual chemosensor for the rapid detection of mercury(ii) pollution and biothiols, Analyst 144 (2019) 4908–4916, https://doi.org/10.1039/C9AN01055F.
[43] M.D. Gholami, F. Thesis, P. Sonar, G.A. Ayoko, E.L. Izake, Rapid and selective detection of recombinant human erythropoietin in human blood plasma by a sensitive optical sensor, Analyst 145 (2020) 5508–5515, https://doi.org/10.1039/D0AN00972E.
[44] M.D. Gholami, P. Sonar, G.A. Ayoko, E.L. Izake, A highly sensitive SERS quenching nanosensor for the determination of tumor necrosis factor alpha in blood, Sens. Actuators, B 310 (2020), 127867, https://doi.org/10.1016/j.snb.2020.127867.
[45] M.D. Gholami, A.P. O'Mullane, P. Sonar, G.A. Ayoko, E.L. Izake, Antibody coated conductive polymer for the electrochemical immunosensing of Human Cardiac Troponin I in blood plasma, Anal. Chim. Acta 1185 (2021), 339082, https://doi.org/10.1016/j.aca.2021.339082.
[46] M.D. Gholami, P. Sonar, G.A. Ayoko, E.L. Izake, A SERS quenching method for the sensitive determination of insulin, Drug Test. Anal. 13 (2021) 1048–1053, https://doi.org/10.1002/dta.2808.
[47] Q. Guo, Y. Zhang, Z.H. Lin, Q.Y. Cao, Y. Chen, Fluorescent norbornene for sequential detection of mercury and biothiols, Dyes Pigments 172 (2020), 107872, https://doi.org/10.1016/j.dyepig.2019.107872.
[48] R.L. Pinals, F. Ledesma, D. Yang, N. Navarro, S. Jeong, J.E. Pak, L. Kuo, Y. C. Chuang, Y.W. Cheng, H.Y. Sun, M.P. Landry, Rapid SARS-CoV-2 spike protein detection by carbon nanotube-based near-infrared nanosensors, Nano Lett. 21 (2021) 2272–2280, https://doi.org/10.1021/acs.nanolett.1c00118.
[49] K.K.W. To, O.T.Y. Tsang, W.S. Leung, A.R. Tam, T.C. Wu, D.C. Lung, C.C.Y. Yip, J. P. Cai, J.M.C. Chan, T.S.H. Chik, D.P.L. Lau, C.Y.C. Choi, L.L. Chen, W.M. Chan, K. H. Chan, J.D. Ip, A.C.K. Ng, R.W.S. Poon, C.T. Luo, V.C.C. Cheng, J.F.W. Chan, I.F. N. Hung, Z. Chen, H. Chen, K.Y. Yuen, Temporal profiles of viral load in posterior oropharyngeal saliva samples and serum antibody responses during infection by SARS-CoV-2: an observational cohort study, Lancet Infect. Dis. 20 (2020) 565–574, https://doi.org/10.1016/S1473-3099(20)30196-1.
[50] A.L. Wyllie, J. Fournier, A. Casanovas-Massana, M. Campbell, M. Tokuyama, P. Vijayakumar, J.L. Warren, B. Geng, M.C. Muenker, A.J. Moore, C.B.F.M. E. Vogels, I.M. Petrone Ott, P. Lu, A. Venkataraman, A. Lu-Culligan, J. Klein, R. Earnest, M. Simonov, R. Datta, R. Handoko, N. Naushad, L.R. Sewanan, J. Valdez, E.B. White, S. Lapidus, C.C. Kalinich, X. Jiang, D.J. Kim, E. Kudo, M. Linehan, T. Mao, M. Moriyama, J.E. Oh, A. Park, J. Silva, E. Song, T. Takahashi, M. Taura, O.E. Weizman, P. Wong, Y. Yang, S. Bermejo, C.D. Odio, S.B. Omer, C.S. D. Cruz, S. Farhadian, R.A. Martinello, A. Iwasaki, N.D. Grubaugh, A.I. Ko, Saliva or nasopharyngeal swab specimens for detection of SARS-CoV-2, N. Engl. J. Med. 383 (2020) 1283–1286, https://doi.org/10.1056/NEJMc2016359.
[51] X. Zou, Y. Ji, H. Li, Z. Wang, L. Shi, S. Zhang, T. Wang, Z. Gong, Recent advances of environmental pollutants detection via paper-based sensing strategy, Luminescence 36 (2021) 1818–1836, https://doi.org/10.1002/bio.4130.
[52] T.R.L.C. Paixão, C.D. Garcia, Chapter 2 - chemistry of paper-properties, modification strategies, and uses in bioanalytical chemistry, in: W.R. de Araujo, T. R.L.C. Paixão (Eds.), Paper-based Analytical Devices for Chemical Analysis and Diagnostics, Elsevier, 2022, pp. 15–39.
[53] E. Noviana, C.P. McCord, K.M. Clark, I. Jang, C.S. Henry, Electrochemical paper-based devices: sensing approaches and progress toward practical applications, Lab Chip 20 (2020) 9–34, https://doi.org/10.1039/C9LC00903E.
[54] E. Noviana, D.B. Carrão, R. Pratiwi, C.S. Henry, Emerging applications of paper-based analytical devices for drug analysis: a review, Anal. Chim. Acta 1116 (2020) 70–90, https://doi.org/10.1016/j.aca.2020.03.013.
[55] H. Liu, G. Zhao, M. Wu, Z. Liu, D. Xiang, C. Wu, Y. Cheng, H. Wang, Z.L. Wang, L. Li, Ionogel infiltrated paper as flexible electrode for wearable all-paper based sensors in active and passive modes, Nano Energy 66 (2019), 104161, https://doi.org/10.1016/j.nanoen.2019.104161.
[56] S.R. Chinnadayyala, J. Park, H.T.N. Le, M. Santhosh, A.N. Kadam, S. Cho, Recent advances in microfluidic paper-based electrochemiluminescence analytical devices for point-of-care testing applications, Biosens. Bioelectron. 126 (2019) 68–81, https://doi.org/10.1016/j.bios.2018.10.038.
[57] M. Parrilla, T. Guinovart, J. Ferré, P. Blondeau, F.J. Andrade, A wearable paper-based sweat sensor for human perspiration monitoring, Adv. Healthc. Mater. 8 (2019), 1900342, https://doi.org/10.1002/adhm.201900342.